Second-harmonic generation from singular metasurfaces

Fan Yang *

College of Physics, Key Laboratory of High Energy Density Physics and Technology of the Ministry of Education, Sichuan University, Chengdu, Sichuan 610065, China

Cristian Ciracì

Istituto Italiano di Tecnologia, Center for Biomolecular Nanotechnologies, Via Barsanti 14, 73010 Arnesano, Italy

(Received 12 April 2022; revised 31 May 2022; accepted 13 June 2022; published 23 June 2022)

We present a theoretical study of second-harmonic generation from a singular metasurface. The singular metasurfaces strongly interact with the incident light, where the large field enhancement forms an intense surface polarization that generates the second-harmonic field. By using transformation optics, the calculation of nonlinear optical response is converted from the metasurface frame to that of a simple slab geometry, largely reducing the complexity of the problem. In addition, the singular metasurface exhibits a weak dependence on the incident angle of light, which can be potentially used as an all-angle device for harmonic generations. Finally, we study the symmetry dependence of second-harmonic generation in the far field for the singular metasurface and show how to enhance the conversion efficiency under normal incidence by breaking the surface inversion symmetry.

DOI: 10.1103/PhysRevB.105.235432

I. INTRODUCTION

Optical nonlinear effects [1,2] have received considerable interest since the discovery of second-harmonic generation (SHG) in 1961 [3]. With the development of nanofabrication processes in past decades, nanoscale structures have become an important component in nonlinear optics. Unlike traditional nonlinear crystals, nanostructured materials can provide strong light–matter interaction and simultaneously relax the phase-matching condition constraint [4,5]. Nanostructures may be classified into two groups: All-dielectric and plasmonic systems [6–8]. All-dielectric nanostructures utilize both electric and magnetic resonances, whose excitation can contribute to an efficient harmonic generation [9,10]. In contrast, plasmonic structures take advantage of the excitation of surface plasmon polaritons, creating a strong field enhancement at the metal surface. This strong field then gives rise to a large nonlinear optical response [11] in a close by dielectric [12] or in the metal itself [13] through the dynamics of free electrons [14,15]. Hybrid metal-dielectric resonators have also been proposed [16].

Many scenarios have been suggested to further enhance the nonlinear response of nanostructures. For instance, the application of the epsilon-near-zero (ENZ) concept boosts the nonlinear response [17–19]. Alam *et al.* have shown that ITO films display ENZ properties at near-infrared frequencies, leading to a giant Kerr nonlinearity [19]. The concept of bound state in the continuum (BIC) [20] has also been employed to greatly enhance SHG because the excitation of BIC contributes to a large quality factor [21,22]. Another method to further enhance the nonlinear effect is introducing a singularity in the nanostructure. A singularity can be an ultrasmall gap between two metallic interfaces or a sharp metallic tip [23]. These singular structures exhibit a much stronger field enhancement than conventional plasmonic structures, so a giant nonlinear response is expected near the singularities. The nonlinearity enhancement by singularities has been confirmed in a variety of experiments, such as nanoparticle dimers [24], bowtie antennas [11], particles on metal surface [25], etc.

Even though nonlinear nanophotonics have received substantial attention for a few decades, most research relies on experimental measurements and numerical simulations. Only a few works give analytic solutions to the nonlinear optical response of nanostructures, such as flat surface, cylinder, and sphere [26–28].

In the past decade, transformation optics have been successfully applied in the field of plasmonics, providing the tools to convert calculations for a complex nanostructure into a simple slab geometry problem [23,29]. After obtaining the analytical solution in the slab frame, it is in fact possible to derive the corresponding field profile of the nanostructure by mapping the fields between two frames. Recently, this powerful analytical tool has been utilized to study the SHG from a kissing nanowire dimer [30,31]. However, a transformation optics approach to extended structures such as a metasurface has not been explored yet.

Based on our previous work about the linear optical response of singular metasurfaces [32], in this article we analytically investigate the SHG process in analogous systems. In particular, we consider the nonlinear response of free electrons at the metal surface [33,34]. We show that the intense field enhancement in the singular metasurface provides a strong nonlinear excitation for the second-harmonic field. In addition, the singular metasurface supports a hidden dimension that enables a continuous mode excitation when changing the k vector of incident waves [35], thereby leading

*fyang@scu.edu.cn

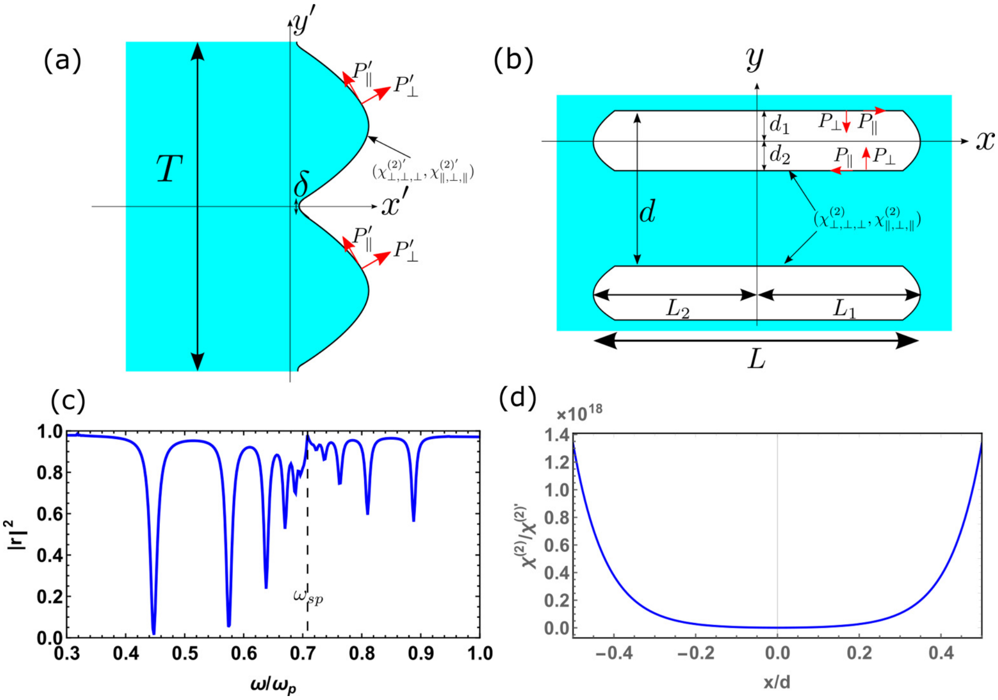

FIG. 1. Mapping of nonlinearity. (a) The geometry of the singular metasurface with the singularity scaled by δ. The period is T. (b) The corresponding slab frame and the nonlinear surface polarization, where the slab period is d and the cavity length is L. (c) The linear reflection spectrum of a singular metasurface, where the incident angle θ_{in} of the plane wave is $\pi/4$. (d) The nonlinear surface susceptibility $\chi^{(2)}$ in the slab frame. The geometric parameter settings in panels (c) amd (d) are $T = 10$ nm, $\theta = 0.2\pi$, $d_1 = d_2 = 0.05d$, and $L = d = 1$.

to an all-angle high SHG efficiency. Finally, the singular metasurface possesses a few surface symmetries that strongly affect SHG efficiency in the far field.

II. MAPPING OF NONLINEARITY

The singular metasurface investigated in this paper is shown in Fig. 1(a). The metasurface considered here has a period T along the y' axis and a translation invariance along the z' axis. For practical consideration, the sharp singular point is scaled by the width δ. We consider the singular metasurface made up of a centrosymmetric plasmonic material [cyan region in Fig. 1(a)] parameterized with a Drude model $\varepsilon = 1 - \omega_p^2/(\omega^2 + i\omega\gamma)$, where $\omega_p = 1.36\times10^{16}$ rad/s and $\gamma = 1\times10^{14}$ rad/s. In a centrosymmetric medium, the second-order nonlinear process is not allowed [1]. However, the inversion symmetry can be broken at the material surface. It is reasonable then to define a surface second-order nonlinear susceptibility. The nonlinear optical response of a plasmonic material can be described by the hydrodynamic model, which is simple but accurate in the description of nonlinear optical response near the metallic surface [33]. We assume that all nonlinear contributions come from the metal surface [30]. Applying this approximation in hydrodynamic model, the two nonzero surface susceptibilities can be written as [33]

$$\chi^{(2)'}_{\perp\perp\perp} = -\frac{\varepsilon_0}{4n_0 e}\frac{3\omega_F + i\gamma}{2\omega_F + i\gamma}(\varepsilon_F - 1)^2$$
$$\chi^{(2)'}_{\parallel\perp\parallel} = -\frac{\varepsilon_0}{2n_0 e}(\varepsilon_F - 1)^2, \quad (1)$$

where ε_F is the relative permittivity at fundamental pump frequency ω_F, ε_0 is the free space permittivity, $n_0 = 5.7\times10^{28}$ m^{-3} is the equilibrium charge density, and $-e$ is the electron charge [33]. The prime denotes the physical quantity in the metasurface frame, i.e., Fig. 1(a), and the two nonlinear surface polarizations can be expressed in the form

$$P'_{\perp} = \varepsilon_0 \chi^{(2)'}_{\perp\perp\perp} E'^2_{\perp}$$
$$P'_{\parallel} = \varepsilon_0 \chi^{(2)'}_{\parallel\perp\parallel} E'_{\perp} E'_{\parallel}, \quad (2)$$

where $E'_{\perp}$ ($E'_{\parallel}$) is the electric field normal (parallel) to the metal interface at fundamental frequency ω_F, which is evaluated at the point immediately inside the metal interface [26]. The direction of $P'_{\perp}$ and $P'_{\parallel}$ is denoted in Fig. 1(a), shown as red arrows. These two polarizations can be linked with two surface currents: The electric surface current $J^{e'}$ and the magnetic surface current $J^{m'}$. Their relations are [36,37]

$$J^{m'} = \frac{1}{\varepsilon_b}\mathbf{n} \times \nabla_{\parallel} P'_{\perp}$$
$$J^{e'} = \frac{\partial P'_{\parallel}}{\partial t}, \quad (3)$$

where ε_b is the background permittivity experienced by $P'_{\perp}$, and $J^{m'}$ and $J^{e'}$ are along the parallel direction. The origins of these two surface currents are the induced electric surface polarizations, where the parallel component contributes to the common electric surface current, while the normal one (a dipole layer) gives rise to an effective magnetic surface current. In our surface polarization model, the background permittivity experienced by the induced polarization at second-harmonic frequency ω_S is $\varepsilon_0\varepsilon_S$ [33], where ε_S is the metal permittivity at frequency ω_S.

According to Eq. (2), the fundamental field oscillating at frequency ω_F generates, through the second-order process, a nonlinear source that in turn gives rise to a pair of surface polarization components ($P'_\perp, P'_\parallel$). These two polarizations lead to the following boundary conditions at the second-harmonic frequency ω_S [36,37],

$$\begin{aligned} E'^{+}_{\parallel} - E'^{-}_{\parallel} &= -J^{m'}_z = -\frac{ik'_\parallel}{\varepsilon_b}P'_\perp \\ H'^{+}_z - H'^{-}_z &= -J^{e'}_\parallel = i\omega_S P'_\parallel, \end{aligned} \tag{4}$$

where the superscript + (−) represents the point immediately outside (inside) the metal interface.

Now we are going to map the above boundary conditions to the slab frame in Fig. 1(b). A singular metasurface with blunt singular points in Fig. 1(a) can be mapped to a periodic slab system with the period d in the y direction and the finite cavity length L shown in Fig. 1(b) by following conformal mapping [32],

$$z = \frac{d}{2\pi}\ln\left(\frac{2}{e^{2\pi z'/T} - 1)} + 1\right), \tag{5}$$

where $z = x + iy$ and $z' = x' + iy'$ are complex coordinates in the slab frame and the metasurface frame, respectively. When the size of singularity vanishes, the cavity length L diverges, i.e., an infinite cavity.

From the rule of transformation optics, electric-field $E'_\parallel$ and k-vector $k'_\parallel$ have been stretched by the same factor $1/\sqrt{\det(\Lambda)}$ when mapping from the metasurface frame in Fig. 1(a) to slab frame in Fig. 1(b) [38,39]. Here $\det(\Lambda)$ is the Jacobian matrix whose elements are defined as $\Lambda_{ij} = \frac{\partial x'_i}{\partial x_j}$. Transformation optics preserves the validity of electromagnetic boundary condition when mapping from the physical space to the transformed space. Therefore according to Eq. (4), the surface polarization $P'_\perp$ is conserved when transforming from the metasurface frame to the slab frame. On the other hand, the z component of magnetic-field H'_z is also conserved under the transformation, leaving the other surface polarization $P_\parallel$ unchanged as well. Since the surface polarization $P'_{\perp,\parallel}$ is a conserved quantity, we have

$$\begin{aligned} P'_\perp &= \varepsilon_0\chi^{(2)'}_{\perp\perp\perp}E'^2_\perp = \varepsilon_0\chi^{(2)'}_{\perp\perp\perp}\frac{E^2_\perp}{\det(\Lambda)} = \varepsilon_0\chi^{(2)}_{\perp\perp\perp}E^2_\perp = P_\perp \\ P'_\parallel &= \varepsilon_0\chi^{(2)'}_{\parallel\perp\parallel}E'_\perp E'_\parallel = \varepsilon_0\chi^{(2)'}_{\parallel\perp\parallel}\frac{E_\perp E_\parallel}{\det(\Lambda)} = \varepsilon_0\chi^{(2)}_{\parallel\perp\parallel}E_\perp E_\parallel = P_\parallel \end{aligned} \tag{6}$$

from which the transformation rule of the surface nonlinear susceptibility $\chi^{(2)}_{\perp\perp\perp,\parallel\perp\parallel}$ can be written as

$$\begin{aligned} \chi^{(2)}_{\perp\perp\perp,\parallel\perp\parallel} &= \frac{\chi^{(2)'}_{\perp\perp\perp,\parallel\perp\parallel}}{\det(\Lambda)} \\ &= \chi^{(2)'}_{\perp\perp\perp,\parallel\perp\parallel}\left|\frac{dz}{dz'}\right|^2 \\ &= \chi^{(2)'}_{\perp\perp\perp,\parallel\perp\parallel}\left(\frac{d}{T}\left|\sinh\left(\frac{2\pi}{d}z\right)\right|\right)^2, \end{aligned} \tag{7}$$

which is coordinate dependent in the slab frame. In this frame, the metal-air interfaces are located at $y = d_1$ and $y = -d_2$. Therefore the surface nonlinear susceptibility in the slab frame is a function of x, shown in Fig. 1(d).

III. INDUCED SURFACE POLARIZATION

In the above section, we have demonstrated that the surface polarization conserves under the transformation from the metasurface to the slab geometries. Thus the nonlinear surface polarization profile $P'_{\perp,\parallel}(x', y')$ along the interface of metasurface can be obtained by directly mapping $P_{\perp,\parallel}(x, y)$ from the slab frame, which can be evaluated by using Eq. (6). The electric-field profile of $E_{\perp,\parallel}$ and $E'_{\perp,\parallel}$ can be found in our previous linear response theory [32]. In Fig. 2, the distribution of electric field at the interface $E'_{\perp,\parallel}$ and the induced polarization $P'_{\perp,\parallel}$ are shown. The singular metasurface supports two kinds of modes with different symmetries: The a_x (a_y) mode below (above) ω_{sp} in the reflection spectrum in Fig. 1(c) [32]. In the first column in Fig. 2, we illustrate a_x and a_y modes in panels (a) and (b), respectively, where the a_x (a_y) mode is excited by the parallel (normal) electric-field component. In the reflection spectrum, the resonance peaks correspond to the excitation of a few discrete modes, which merge into a continuous spectrum when the width of singularity $\delta \to 0$ [32]. Because an exact singular point corresponds to an infinite slab system, the modes are excited in a continuous manner [35]. In Fig. 2(a), we study the a_x mode whose electric field is antisymmetric for the normal field component $E'_\perp$ while symmetric for the tangential component $E'_\parallel$. As a comparison, the electric field of the a_y mode shown in Fig. 2(b) exhibits the opposite symmetry for the corresponding normal and tangential field components.

From the definition in Eq. (2), the nonlinear surface polarization $P'_\perp$ is a quadratic function of electric-field $E'_\perp$. Despite the different symmetry of the electric-field $E'_\perp$ for a_x and a_y modes in Figs. 2(a) and 2(b), the surface polarization $P'_\perp$ of these two modes are both symmetric (an even function of y'). For the other surface polarization $P'_\parallel$, the results in Fig. 2 shows that both a_x and a_y modes have antisymmetric property (an odd function of y'). This can be explained by observing that the electric fields $E'_\perp$ and $E'_\parallel$ share different symmetries for both a_x and a_y modes, so the product of these two fields ($\propto P'_\parallel$) remains antisymmetric.

In the right two columns in Fig. 2, the two nonlinear surface polarizations $P'_\perp$ and $P'_\parallel$ are projected on x and y axes, respectively. We observe that the x component is symmetric, while the y component is antisymmetric. In the following text, we show that the symmetry of these surface polarizations strongly affects the SHG in the far field.

IV. INDUCED BULK POLARIZATION

The induced nonlinear surface polarization becomes a source excitation at the second-harmonic frequency ω_S. In order to provide an analytical solution for the excited second-harmonic field, we implement the calculation in the slab frame shown in Fig. 1(b). The surface polarization at the metal-dielectric interface in the slab frame varies along the

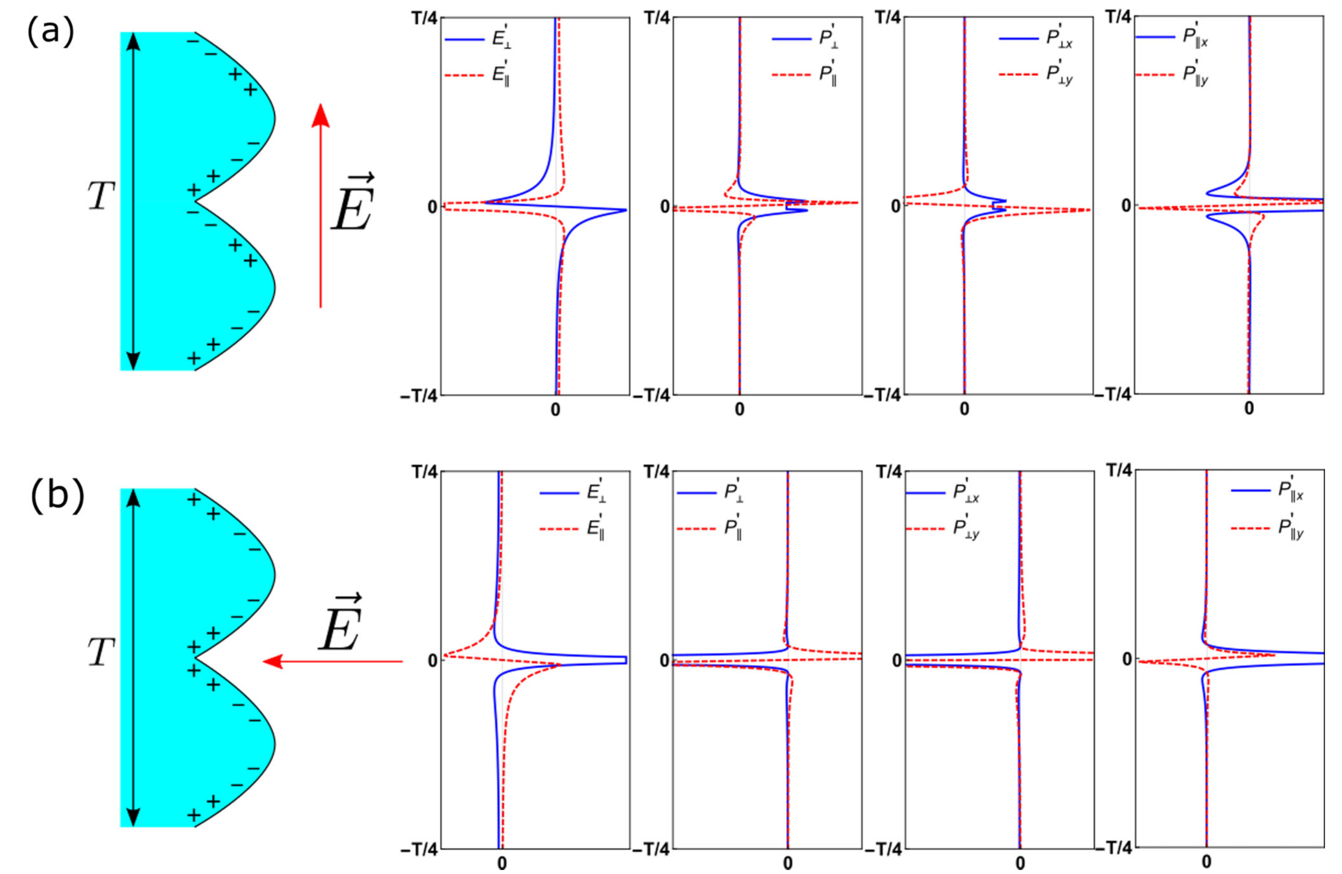

FIG. 2. Surface polarization of singular metasurface with period $T = 10$ nm, vertex angle $\theta = 0.2\pi$, $d_1 = d_2 = 0.05d$, $L = d = 1$, and $\theta_{in} = \pi/4$.(a) a_x mode excited by the parallel electric component (red arrow) at $\omega = 0.449\omega_p$ and the corresponding electric field and induced nonlinear surface polarization; (b) a_y mode excited by the electric field normal to the metasurface (red arrow) at $\omega = 0.888\omega_p$ and the corresponding electric field and induced nonlinear surface polarization.

x direction, which can be expanded as a Fourier series

$$P_{\perp,\parallel} = \sum_{n=-\infty}^{\infty} P^n_{\perp,\parallel} e^{ik_n x}. \tag{8}$$

With this mode expansion of the source excitation, the excited field can also be expanded as $H_z = \sum_{n=-\infty}^{\infty} H_z^n e^{ik_n x}$, where the mode k_n in the slab frame can be expressed as

$$H_z^n(k_n, y) = \begin{cases} b_+ e^{-\sqrt{k_n^2}y} + b_- e^{\sqrt{k_n^2}y}, & -d_2 < y < d_1 \\ c_+ e^{-\sqrt{k_n^2}y} + c_- e^{\sqrt{k_n^2}y}, & -(d_2+d_3) < y < -d_2 \end{cases} \tag{9}$$

and the corresponding tangential electric field is

$$E_x^n(k_n, y) = \begin{cases} -\frac{i\sqrt{k_n^2}}{\omega_S\varepsilon_0}(b_+ e^{-\sqrt{k_n^2}y} - b_- e^{\sqrt{k_n^2}y}), & -d_2 < y < d_1 \\ -\frac{i\sqrt{k_n^2}}{\omega_S\varepsilon_0\varepsilon_S}(c_+ e^{-\sqrt{k_x^2}y} - c_- e^{\sqrt{k_n^2}y}), & -(d_2+d_3) < y < -d_2. \end{cases} \tag{10}$$

The excited mode coefficients $b_\pm$ and $c_\pm$ can be obtained by imposing the following boundary conditions for the second-harmonic near-field

$$\begin{aligned} H_z^{n+} - H_z^{n-}\big|_{y=-d_2} &= J_x^e\big|_{y=-d_2} = i\omega_S P_\parallel^n|_{y=-d_2} \\ H_z^{n+} - H_z^{n-}\big|_{y=d_1} &= -J_x^e\big|_{y=d_1} = i\omega_S P_\parallel^n|_{y=d_1} \\ E_x^{n+} - E_x^{n-}\big|_{y=-d_2} &= J_z^m\big|_{y=-d_2} = -\frac{ik_n}{\varepsilon_0\varepsilon_S}P_\perp^n|_{y=-d_2} \\ E_x^{n+} - E_x^{n-}\big|_{y=d_1} &= -J_z^m\big|_{y=d_1} = -\frac{ik_n}{\varepsilon_0\varepsilon_S}P_\perp^n|_{y=d_1} \end{aligned} \tag{11}$$

from which we obtain the following system of equation in the matrix form

$$\begin{pmatrix} e^{|k_n|d_2} & e^{-|k_n|d_2} & -e^{|k_n|d_2} & -e^{-|k_n|d_2} \\ e^{-|k_n|d_1} & e^{|k_n|d_1} & -e^{|k_n|(d_2+d_3)} & -e^{-|k_n|(d_2+d_3)} \\ |k_n|e^{|k_n|d_2} & -|k_n|e^{-|k_n|d_2} & -|k_n|e^{|k_n|d_2}/\varepsilon_S & |k_n|e^{-|k_n|d_2}/\varepsilon_S \\ |k_n|e^{-|k_n|d_1} & -|k_n|e^{|k_n|d_1} & -|k_n|e^{|k_n|(d_2+d_3)}/\varepsilon_S & |k_n|e^{-|k_n|(d_2+d_3)}/\varepsilon_S \end{pmatrix}\begin{pmatrix} b_+ \\ b_- \\ c_+ \\ c_- \end{pmatrix} = \begin{pmatrix} i\omega_S P_\parallel^n|_{y=-d_2} \\ i\omega_S P_\parallel^n|_{y=d_1} \\ \frac{\omega_S k_n}{\varepsilon_S} P_\perp^n|_{y=-d_2} \\ \frac{\omega_S k_n}{\varepsilon_S} P_\perp^n|_{y=d_1} \end{pmatrix}. \tag{12}$$

By solving the above system of equation, we obtain the excited near field by the surface polarization at ω_S. In Figs. 3(a) and 3(b), we show the profile of near field and polarization for a_x and a_y modes, respectively. From Fig. 2 it can be observed that the nonlinear surface polarizations for a_x and a_y modes have the same kind of symmetry, thereby inducing the same symmetry for near field and polarization in Fig. 3. In the linear optical response [32], the singular metasurface supports a giant field enhancement near the singularities. As expected, the singular points also generate hot spots for the second-harmonic field, because a singular point can adiabatically compress the wavelength of surface plasmon at ω_S, leading to a high density of states and a strong field enhancement near the singularities.

V. FROM NEAR FIELD TO FAR FIELD

The induced surface polarization and near field at second-harmonic frequency are obtained in the previous section. The near field gives rise to an effective surface polarization macroscopically, which can be obtained by averaging the polarization in one period. Here the grating period is assumed to be subwavelength so that the higher diffraction order can be ignored. In this approximation, the k vector of the second-harmonic field parallel to the metasurface is $k_{0y}^{\omega_S} = 2k_{0y}^{\omega_F}$. This macroscopic surface polarization has two origins: One is from the surface polarization $P'_{\perp,\parallel}$ defined in Eq. (2), while the other one is from the bulk polarization induced by $P'_{\perp,\parallel}$.

The application of transformation optics enables the calculation of these polarizations in the slab frame where the analytic calculation becomes possible. Let us first discuss the contribution from nonlinear surface polarization $P'_{\perp,\parallel}$, whose contribution to the effective surface polarization can be calculated by

$$\begin{aligned}\overline{P'_{x1}} &= \frac{1}{T}\int P'_x dl' = \frac{1}{T}\left(\int P'_\perp dy' + \int P'_\parallel dx'\right)\\ &= \frac{1}{T}\left(\int P_\perp dy' + \int P_\parallel dx'\right)\\ \overline{P'_{y1}} &= \frac{1}{T}\int P'_y dl' = \frac{1}{T}\left(\int -P'_\perp dx' + \int P'_\parallel dy'\right)\\ &= \frac{1}{T}\left(\int -P_\perp dx' + \int P_\parallel dy'\right),\end{aligned} \tag{13}$$

where the line integration is along the metasurface interface, and the quantity with overline stands for the effective surface polarization. Then, by using the chain rule and Cauchy-Riemann conditions, we have

$$\begin{aligned}\overline{P'_{x1}} &= \frac{1}{T}\int \left(-P_\perp \frac{\partial x'}{\partial y} + P_\parallel \frac{\partial x'}{\partial x}\right) dx\\ \overline{P'_{y1}} &= \frac{1}{T}\int \left(-P_\perp \frac{\partial x'}{\partial x} - P_\parallel \frac{\partial x'}{\partial y}\right) dx.\end{aligned} \tag{14}$$

The other contribution to the effective surface polarization is the induced bulk polarization in the metallic region at second-harmonic frequency ω_S, which can be integrated as

$$\begin{aligned}\overline{P'_{x2}} &= \frac{1}{T}\iint_{\text{metal}} P'_x dx' dy'\\ \overline{P'_{y2}} &= \frac{1}{T}\iint_{\text{metal}} P'_y dx' dy'.\end{aligned} \tag{15}$$

Since the transformation of bulk polarization follows [40]

$$\begin{pmatrix} P'_x \\ P'_y \end{pmatrix} = \frac{1}{\det(\Lambda)}\begin{pmatrix} \frac{\partial x'}{\partial x} & \frac{\partial x'}{\partial y} \\ -\frac{\partial x'}{\partial y} & \frac{\partial x'}{\partial x} \end{pmatrix}\begin{pmatrix} P_x \\ P_y \end{pmatrix} \tag{16}$$

and the bulk region integration follows [41],

$$\iint_{\text{metal}} dx'dy' = \iint_{\text{metal}} \det(\Lambda) dx dy. \tag{17}$$

Therefore we obtain the following integration formulas to calculate the contribution of bulk polarization to the effective surface polarization of the metasurface, which reads

$$\begin{aligned}\overline{P'_{x2}} &= \frac{1}{T}\iint_{\text{metal}} \left(\frac{\partial x'}{\partial x}P_x + \frac{\partial x'}{\partial y}P_y\right) dx dy\\ \overline{P'_{y2}} &= \frac{1}{T}\iint_{\text{metal}} \left(-\frac{\partial x'}{\partial y}P_x + \frac{\partial x'}{\partial x}P_y\right) dx dy.\end{aligned} \tag{18}$$

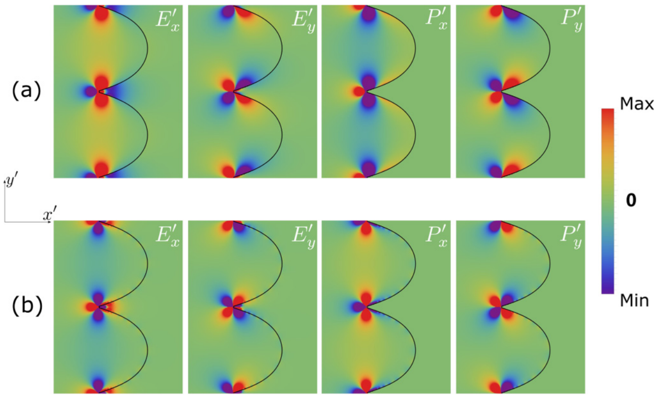

FIG. 3. Excited near field in the second-harmonic frequency ω_S for a singular metasurface with period $T = 10$ nm, vertex angle $\theta = 0.2\pi$, $d_1 = d_2 = 0.05d$, $L = d = 1$, and $\theta_{in} = \pi/4$. (a) Electric field and polarization profile for a_x mode; (b) electric field and polarization profile for a_y mode.

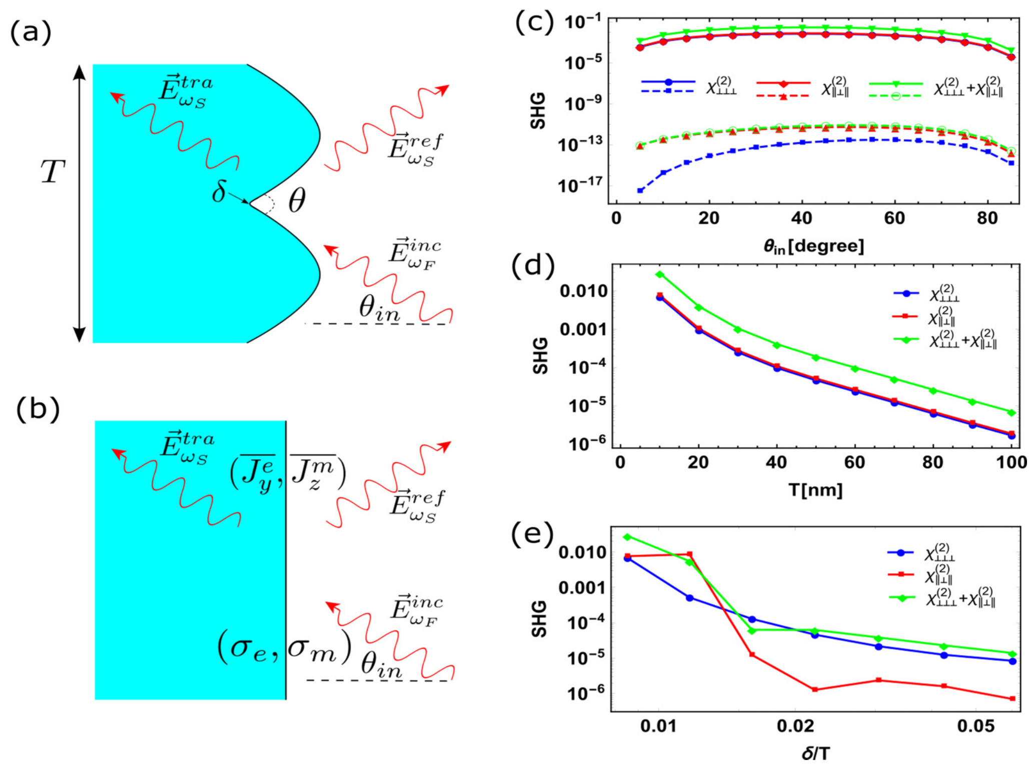

FIG. 4. Far-field calculation for the singular metasurface. (a) The pump field at fundamental frequency ω_F excites SHG in the far field at ω_S; (b) simplified flat surface geometry for SHG calculation, where the nonlinear source is modeled as two current source $(\overline{J^e_y}, \overline{J^m_z})$; (c) the dependence of SHG on incident angle of plane-wave θ_{in} for singular metasurface with $T = 10$ nm, $\theta = 0.2\pi$, $d_1 = d_2 = 0.05d$, and $L = d = 1$; (d) the dependence of SHG on period of metasurface T, where $\theta = 0.2\pi$, $d_1 = d_2 = 0.05d$, $L = d = 1$ and $\theta_{in} = \pi/4$; (e) the dependence of SHG on size of singularity δ with period $T = 10$ nm, where $\theta = 0.2\pi$, $d_1 = d_2 = 0.05d$, and $\theta_{in} = \pi/4$.

The above two contributions can be summed up to form a total surface polarization

$$\overline{P'_x} = \overline{P'_{x1}} + \overline{P'_{x2}}$$
$$\overline{P'_y} = \overline{P'_{y1}} + \overline{P'_{y2}} \tag{19}$$

from which an effective electric surface current and magnetic surface current can be obtained by

$$\overline{J^m_z} = \frac{ik^{\omega_S}_{0y}}{\varepsilon_0}\overline{P'_x}$$
$$\overline{J^e_y} = -i\omega_S\overline{P'_y}. \tag{20}$$

Here the background permittivity experienced by $\overline{P'_x}$ is ε_0.

We can now analyze how the symmetry of induced surface polarization $P'_{\perp,\parallel}$ and bulk polarization $P'_{x,y}$ affects the effective macroscopic surface polarization and current. The projection of $P'_{\perp,\parallel}$ along the x direction is an even function (see Fig. 2) whose average in a period gives a nonzero effective polarization $\overline{P'_{x1}} \neq 0$. On the other hand, the projection along the y direction of the surface polarization $P'_{\perp,\parallel}$ is an odd function, resulting in a zero effective polarization contribution, $\overline{P'_{y1}} = 0$. Similarly, the bulk polarization in Fig. 3 also demonstrates that P'_x is even while P'_y is odd, resulting in $\overline{P'_{x2}} \neq 0$ and $\overline{P'_{y2}} = 0$. Therefore the total effective surface polarization is nonzero for $\overline{P'_x}$ but zero for $\overline{P'_y}$. Then from the relation between surface current and polarization in Eq. (20), we conclude that the second-order nonlinear effect in singular metasurface gives a nonzero effective magnetic surface current but a zero electric current.

The effective surface currents generate a second-harmonic wave in the far field, shown in Fig. 4(a). Assuming the grating period is subwavelength, the metasurface at ω_S can be simplified as a flat metal surface with a pair of surface current $(\overline{J^e_y}, \overline{J^m_z})$ and a pair of surface conductivity (σ_e, σ_m) (electric and magnetic), see Fig. 4(b), where the calculation of two surface conductivities is given in linear response theory of singular metasurface [32]. These two surface conductivities are utilized to model the energy dissipation by the excited plasmonic mode on the metasurface. The generated far field is expressed as

$$H^{\omega_S}_z = \begin{cases} r^{\omega_S} H_0 e^{ik^{\omega_S}_{0x}x + ik^{\omega_S}_{0y}}, & x > 0 \\ t^{\omega_S} H_0 e^{-ik'^{\omega_S}_{0x}x + ik^{\omega_S}_{0y}}, & x < 0, \end{cases} \tag{21}$$

where r^{ω_S} and t^{ω_S} are defined as the coefficients for reflected and transmitted second-harmonic fields, respectively. Since the metasurface studied in this paper is semi-infinite, we only consider a reflected second-harmonic field, whose generation efficiency is $|r^{\omega_S}|^2$. By matching the tangential field $H^{\omega_S}_z$ and $E^{\omega_S}_y$ at the interface $x = 0$ in Fig. 4(b), we arrive at

$$\begin{pmatrix} 1 & -1 \\ Z_a & Z_m \end{pmatrix}\begin{pmatrix} r^{\omega_S} H_0 \\ t^{\omega_S} H_0 \end{pmatrix} = -\begin{pmatrix} \overline{J^e_y} \\ \overline{J^m_z} \end{pmatrix} - \begin{pmatrix} \frac{\sigma_e Z_a}{2} & -\frac{\sigma_e Z_m}{2} \\ \frac{\sigma_m}{2} & \frac{\sigma_m}{2} \end{pmatrix}\begin{pmatrix} r^{\omega_S} H_0 \\ t^{\omega_S} H_0 \end{pmatrix} \tag{22}$$

where $Z_a = \frac{k_{0x}^{\omega_S}}{\omega_S \varepsilon_0}$ and $Z_m = \frac{k_{0x}'^{\omega_S}}{\omega_S \varepsilon_0 \varepsilon_S}$. After some algebraic manipulation, we obtain

$$\begin{pmatrix} r^{\omega_S} H_0 \\ t^{\omega_S} H_0 \end{pmatrix} = -\begin{pmatrix} 1 + \frac{\sigma_e Z_a}{2} & -\left(1 + \frac{\sigma_e Z_m}{2}\right) \\ Z_a + \frac{\sigma_m}{2} & Z_m + \frac{\sigma_m}{2} \end{pmatrix}^{-1} \begin{pmatrix} \overline{J_y^e} \\ \overline{J_z^m} \end{pmatrix} \tag{23}$$

and the SHG efficiency is

$$|r^{\omega_S}|^2 = \left| \frac{2\left(\overline{J_z^m}(2+Z_m\sigma_e)+\overline{J_y^e}(2Z_m+\sigma_m)\right)}{4(Z_a+Z_m + Z_a Z_m \sigma_e) + (4+(Z_a + Z_m)\sigma_e)\sigma_m} \right|^2 / |H_0|^2. \tag{24}$$

The SHG from a flat metal surface can be calculated following the same procedure. By setting $\sigma_e = 0$ and $\sigma_m = 0$, we arrive at the SHG by a flat surface

$$|r^{\omega_S}|^2 = \left| \frac{Z_m J_y^e + J_z^m}{Z_m + Z_d} \right|^2 / |H_0|^2, \tag{25}$$

where J_y^e and J_z^m in the case of a flat surface can be obtained straightforwardly by calculating the induced surface polarization. We omit the overline on top of the electric and magnetic surface current because no averaging of surface polarization is required for a flat surface. Details regarding the calculation of a flat metal surface can be found in Appendix B.

In Fig. 4(c), we calculate the SHG efficiency as a function of the incident angle for an incident plane wave of frequency $\omega_F = 0.449\omega_p$, the first resonance peak in Fig. 1(c). Throughout this paper, the pump field is a TM wave with a peak intensity of 55 MW/cm^2. By changing the incidence angle, it is surprising to observe that the SHG shows a quite flat curve (solid lines), which means the SHG of the singular metasurface weakly depends on θ_{in}. Therefore the singular metasurface can realize all-angle SHG. This weak dependence on the incident angle is due to a hidden dimension of the singular metasurface [35]. The additional dimension gives the k vector of the mode one more degree of freedom, making the mode excitation in a continuous manner when changing the incident angle. We have also divided the SHG contribution from the two components of nonlinear surface susceptibility $\chi^{(2)}_{\perp\perp\perp}$ and $\chi^{(2)}_{\parallel\perp\parallel}$. The blue curve corresponds to the case when only $\chi^{(2)}_{\perp\perp\perp}$ is considered, while the red curve refers to the contribution of $\chi^{(2)}_{\parallel\perp\parallel}$. The green curve shows the case when both surface susceptibilities are considered. These theoretical results have also been confirmed with numerical simulation, where the detailed simulation setup and results can be found in Appendixes A and C.

For reference, we compare the SHG from the singular metasurface with the SHG from an unstructured metal surface, i.e., a flat surface. The SHG from a flat surface made up of the same metal as the metasurface is presented in Fig. 4(c) as dashed lines, where three different colors correspond to three kinds of combinations of nonlinear surface susceptibilities. The comparison in Fig. 4(c) proves that the singular metasurface strongly improves the SHG efficiency by 10 orders of magnitude when compared with a flat surface.

In Fig. 4(d), we keep the incident angle at 45 degrees but change the grating period T in the calculation of SHG. In tuning the parameter T, the shape of the metasurface is preserved. These results show that the SHG from a singular metasurface decreases when increasing the grating period. This is expected because the number of singular points reduces in a given area when T increases, leading to weaker harmonic generation.

In the above far-field calculation of SHG, the shape of the singular metasurface preserves such that the ratio of singularity size δ to period T is a constant. The ratio δ/T characterizes the degree of singularity, where $\delta/T \to 0$ gives an ideal singular point [32]. In Fig. 4(e), we study how δ/T affects the SHG in the far field by fixing the grating period T and simultaneously shrinking the size of singular point δ, which corresponds to elongating the cavity length L in the slab frame. The calculation results show that the SHG increases when reducing δ/T and finally diverges as $\delta/T \to 0$. However, both the nonclassical effects from electrons [42] and the experimental imperfection [32] result in a blunt singular point for surface plasmons, which ends up with a finite SHG. Another takeaway emerging from Figs. 4(d) and 4(e) is that the SHG efficiency is determined by the size of the singular point and grating period that we can achieve.

VI. SHG AT NORMAL INCIDENCE

As shown in the previous section, the nonlinear source in the singular metasurface can be modeled as two effective surface currents ($\overline{J_y^e}, \overline{J_z^m}$) with only the magnetic one being nonzero. From the definition in Eq. (20), the effective magnetic surface current is proportional to wave-vector $k_{0y}^{\omega_S}$. Therefore both electric and magnetic surface currents become zero under normal incidence, resulting in a zero harmonic field generation in the far field. This situation is often impractical in experimental setups where instead being able to generate at normal incidence is preferable. Is it then possible to modify the metasurface in order to generate SHG in the far field under normal incidence?

The answer is yes. The singular metasurface shown in Fig. 1(a) possesses two kinds of inversion symmetries along with the interface. To quantify the degree of asymmetry for the singular metasurface, we define two factors: α_L and α_d; α_L is defined as L_1/L in Fig. 1(b), quantifying the asymmetry of two singular points in one period. In contrast, α_d measures the asymmetry of two bumps of singular surface, defined as $\alpha_d = d_1/(d_1 + d_2)$ in Fig. 1(b). Particularly, $\alpha_L = 0.5$ gives two identical singular points, while $\alpha_d = 0.5$ leads to two bumps with the same shape. In Fig. 5(a), we have shown four cases of the singular metasurface: (1) $\alpha_L = 0.5$ and $\alpha_d = 0.5$; (2) $\alpha_L = 0.5$ and $\alpha_d \neq 0.5$; (3) $\alpha_L \neq 0.5$ and $\alpha_d = 0.5$; (4) $\alpha_L \neq 0.5$ and $\alpha_d \neq 0.5$. For the pure symmetric case (1), two kinds of inversion centers are marked as black dashed lines. For the asymmetric bump shape in case (2), the inversion center is the center of the bumped region. In contrast, for asymmetric singular points in case (3), the inversion center locates at the center of the singularity. Finally, when the symmetries of both the pumped region and the singular points are broken, the surface inversion center disappears. Therefore we expect only case (4) without a surface inversion symmetry to contribute an SHG in the far field.

To confirm the above assertion, we calculate the effective surface current and SHG in the parameter space of α_L and α_d. Note that changing the value of α_L and α_d shifts the resonance

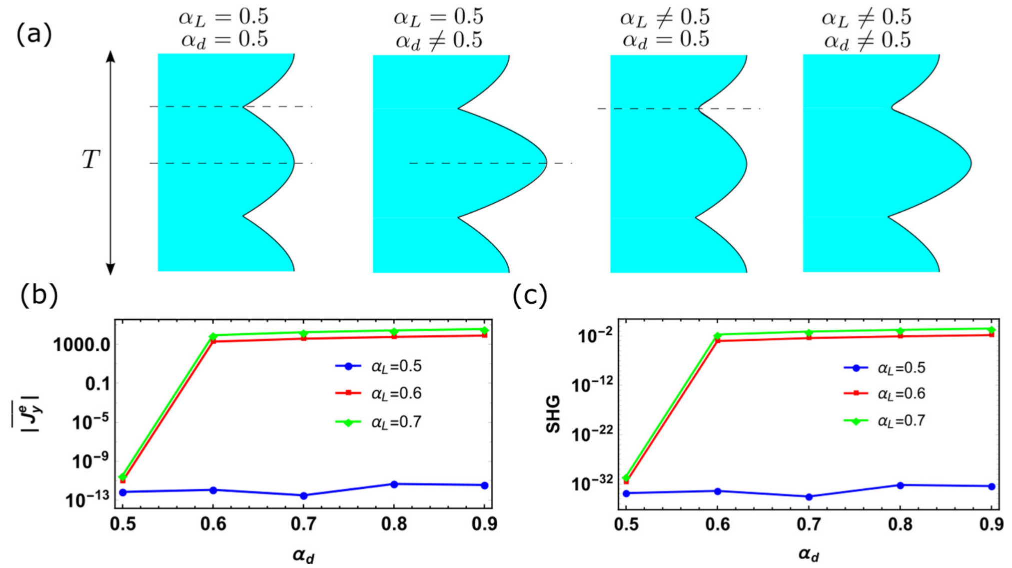

FIG. 5. SHG under normal incidence by breaking the surface inversion symmetry. (a) symmetry of singular metasurface quantified by two parameter α_L and α_d, where dashed line show the inversion center; (b) The effective electric surface current as a function of α_L and α_d; (c) SHG as a function of α_L and α_d. The parameter setting for the singular metasurfaces are $T = 10$ nm and $\theta = 0.2\pi$.

peak position, so we calculate SHG for the corresponding first-order mode. Despite a lack of inversion symmetry, the effective magnetic surface current keeps zero under normal incidence. However, the story differs for the effective electric surface current $\overline{J_y^e}$. Figure 5(b) illustrates the evolution of $\overline{J_y^e}$ in parameter space, which shows that the nonzero effective electric surface can only be achieved by deviating both α_L and α_d from 0.5. The nonzero surface electric current subsequently gives rise to a large SHG in the far field, shown in Fig. 5(c).

VII. CONCLUSION

In conclusion, we have studied the SHG for singular metasurfaces following a transformation optics approach. This work further extends the previous transformation optics-based work about SHG from kissing cylinders to the extended metasurface geometry, bringing new insight into the light–matter interaction for the singular plasmonic structures. By means of transformation optics we have mapped a complex singular surface into a simple slab geometry, such that an analytical solution to SHG can be obtained. Also, the nonlinear source of SHG is modeled as a surface polarization, whose symmetry determines the induced near- and far-field patterns. In addition, the singular metasurface in this paper possesses a variety of symmetries. We show that broken symmetry is necessary to receive a nonlinear far-field signal, which can be realized by using oblique incidence or by breaking the surface inversion symmetry. Finally, we found that SHG of the singular metasurface weakly depends on the incident angle of light, which can be applied to realize an all-angle SHG device.

ACKNOWLEDGMENTS

The authors thank Y. Sivan for useful discussions. F.Y. acknowledges the Fundamental Research Funds for the Central Universities and Science Specialty Program (Grand No. 2020SCUNL210) from Sichuan University.

APPENDIX A: COMSOL SETUP FOR SHG CALCULATION

To check the validity of our theory, we have implemented a Comsol model to perform numerical simulations. We solve a system of two one-way coupled equations for the fundamental and second-harmonic fields, respectively. The critical point in the numerical simulations is the setup of the two surface polarizations $P_\perp$ and $P_\parallel$ in Comsol. Accounting for $P_\parallel$ is straightforward as it is directly related to an electric surface current by $J_\parallel^e = -i\omega_S P_\parallel$, which can be easily implemented using Comsol built-in source options. Considering a surface polarization normal to the interface, on the other hand, is not as simple. In order to account for such a polarization we need to add a weak form contribution. For a bulk polarization vector, $\mathbf{P}_b$, this is $\mu_0\omega_S^2 \int_\Omega \mathbf{P}_b \cdot \tilde{\mathbf{E}} dV$ where $\tilde{\mathbf{E}}$ is the test function and Ω is the volume inside the metal. The relation between a bulk polarization and the surface polarization, $\mathbf{P}$, can be expressed as $\mathbf{P}_b = \delta_{\partial\Omega}\mathbf{P}$, where the delta function $\delta_{\partial\Omega}$ is nonzero only at the metal surface. Finally, for a surface polarization normal to the surface, i.e., $\mathbf{P} = P_\perp \hat{\mathbf{n}}$, we get the following weak form contribution:

$$\mu_0\omega_S^2 \int_{\partial\Omega} P_\perp \tilde{\mathbf{E}} \cdot \hat{\mathbf{n}} dS, \tag{A1}$$

where the integral is now performed only on the metal boundary $\partial\Omega$. Both $P_\perp$ and $\tilde{\mathbf{E}}$ are evaluated inside the metal using the built-in operators *down* or *up*. With this setup in Comsol, we were able to perform numerical simulations of SHG from singular metasurfaces.

APPENDIX B: SHG FROM A FLAT SURFACE

Now, we assume a TM-polarized plane-wave (E_x, E_y, H_z) incident on a flat metallic surface ($x = 0$) from air with incident angle θ_{in}, where $x > 0$ and $x < 0$ correspond to air and metal domain, respectively. The transmitted field inside the metal can be expressed as $H_z^{tra} = tH_0 e^{-ik_{0x}'^{\omega F} x + ik_{0y}^{\omega F} y}$ with

$k_{0y}^{\omega_F} = k_0^{\omega_F} \sin\theta_{in}$, where t is the transmission coefficient for the magnetic field and can be written in terms of incident angle as

$$t = \frac{2\varepsilon_F \cos\theta_{in}}{\varepsilon_F \cos\theta_{in} + \sqrt{\varepsilon_F - \sin^2\theta_{in}}}. \tag{B1}$$

The electric field at ω_F inside the metal ($x < 0$) is

$$E_x = -\frac{k_{0y}^{\omega_F}}{\omega_F \varepsilon_0 \varepsilon_F} t H_0 e^{-ik_{0x}^{\prime\omega_F} x + ik_{0y}^{\omega_F} y}$$

$$E_y = -\frac{k_{0x}^{\prime\omega_F}}{\omega_F \varepsilon_0 \varepsilon_F} t H_0 e^{-ik_{0x}^{\prime\omega_F} x + ik_{0y}^{\omega_F} y}. \tag{B2}$$

From the electric field, the surface polarization can be obtained as

$$P_x = \varepsilon_0 \chi_{\perp\perp\perp}^{(2)} (E_x)^2 = \chi_{\perp\perp\perp}^{(2)} \frac{\left(k_{0y}^{\omega_F}\right)^2}{\omega_F^2 \varepsilon_0 \varepsilon_F^2} t^2 H_0^2 e^{ik_{0y}^{\omega_S} y}$$

$$P_y = \varepsilon_0 \chi_{\parallel\perp\parallel}^{(2)} E_x E_y = \chi_{\parallel\perp\parallel}^{(2)} \frac{k_{0x}^{\prime\omega_F} k_{0y}^{\omega_F}}{\omega_F^2 \varepsilon_0 \varepsilon_F^2} t^2 H_0^2 e^{ik_{0y}^{\omega_S} y}, \tag{B3}$$

where $k_{0y}^{\omega_S} = 2k_{0y}^{\omega_F}$. Finally, the two surface currents can be expressed as

$$J_z^m = i \frac{k_{0y}^{\omega_S}}{\varepsilon_0 \varepsilon_S} \chi_{\perp\perp\perp}^{(2)} \frac{\left(k_{0y}^{\omega_F}\right)^2}{\omega_F^2 \varepsilon_0 \varepsilon_F^2} t^2 H_0^2 e^{ik_{0y}^{\omega_S} y}$$

$$J_y^e = -i\omega_S \chi_{\parallel\perp\parallel}^{(2)} \frac{k_{0x}^{\prime\omega_F} k_{0y}^{\omega_F}}{\omega_F^2 \varepsilon_0 \varepsilon_F^2} t^2 H_0^2 e^{ik_{0y}^{\omega_S} y}. \tag{B4}$$

The generated second-harmonic field can be easily obtained with these two currents by mode matching. The generated second-harmonic fields by the surface current (J_y^e, J_z^m) are expressed as

$$H_z^{ref(\omega_S)} = r^{\omega_S} H_0 e^{ik_{0x}^{\omega_S} x + ik_{0y}^{\omega_S} y}$$

$$H_z^{tra(\omega_S)} = t^{\omega_S} H_0 e^{-ik_{0x}^{\prime\omega_S} x + ik_{0y}^{\omega_S} y}, \tag{B5}$$

where r^{ω_S} and t^{ω_S} are the corresponding coefficients for reflected and transmitted second-harmonic fields. Then by matching the field at the boundary with following boundary

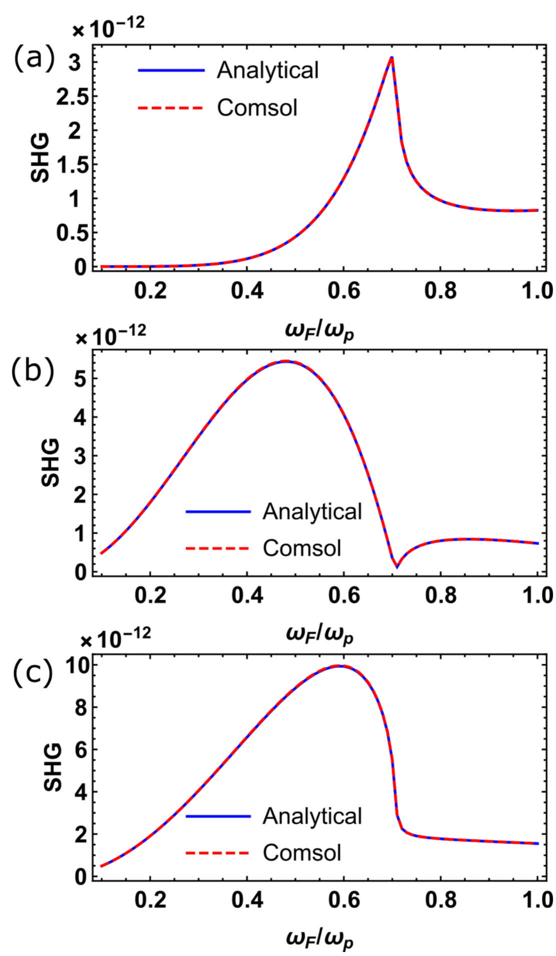

FIG. 6. SHG from a flat metallic surface with incident angle $\theta_{in} = \pi/4$. (a) $\chi_{\perp\perp\perp}^{(2)} \neq 0$ and $\chi_{\parallel\perp\parallel}^{(2)} = 0$; (b) $\chi_{\perp\perp\perp}^{(2)} = 0$ and $\chi_{\parallel\perp\parallel}^{(2)} \neq 0$; (c) $\chi_{\perp\perp\perp}^{(2)} \neq 0$ and $\chi_{\parallel\perp\parallel}^{(2)} \neq 0$. The solid line and the dashed line correspond to theoretical calculation with Eq. (B7) and Comsol simulation, respectively.

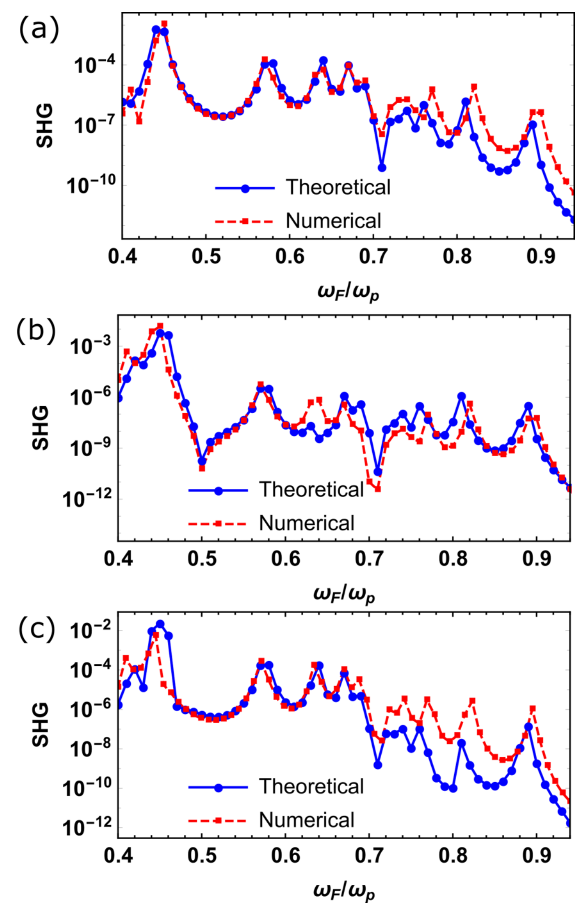

FIG. 7. Numerical verification for theoretical calculation of SHG from singular metasurfaces. (a) $\chi_{\perp\perp\perp}^{(2)} \neq 0$ and $\chi_{\parallel\perp\parallel}^{(2)} = 0$; (b) $\chi_{\perp\perp\perp}^{(2)} = 0$ and $\chi_{\parallel\perp\parallel}^{(2)} \neq 0$; (c) $\chi_{\perp\perp\perp}^{(2)} \neq 0$ and $\chi_{\parallel\perp\parallel}^{(2)} \neq 0$. The solid line and the dashed line correspond to theoretical calculation with Eq. (24) and Comsol simulation, respectively. The geometric parameter settings for the singular metasurface are $T = 10$ nm, $\theta = 0.2\pi$, and $d_1 = d_2 = 0.05d$. The incident angle of the plane wave is $\pi/4$.

conditions

$$H_z^{\omega_s+} - H_z^{\omega_s-} = -J_y^e$$
$$E_y^{\omega_s+} - E_y^{\omega_s-} = -J_z^m, \tag{B6}$$

we have the following SHG efficiency for the flat metal surface

$$|r^{\omega_s}|^2 = \left| \frac{Z_m J_y^e + J_z^m}{Z_m + Z_d} \right|^2 / |H_0|^2. \tag{B7}$$

As a benchmark, we check the theoretical calculation of SHG efficiency of a flat metal surface by Eq. (B7) with Comsol simulation in Fig. 6, where three combinations of two surface susceptibility are considered. The excellent agreement between theory and simulation demonstrates the correctness of our theoretical approach.

APPENDIX C: NUMERICAL VERIFICATION

Using the Comsol simulation, we further check the correctness of our theoretical calculations. Here we compare the frequency dependence of SHG (as a function of fundamental frequency ω_F) between theory and simulation. In Fig. 7, we compare our theory with Comsol results, where a good agreement is achieved. A small discrepancy comes from neglecting the integration of the polarization in the region $x > L_1$ and $x < -L_2$ in the slab frame. The agreement between our theoretical calculation and Comsol simulation confirms the validity of our analytical framework on SHG from a singular metasurface.

[1] R. W. Boyd, *Nonlinear Optics* (Academic Press, San Diego, 2020).

[2] Y.-R. Shen, *Principles of Nonlinear Optics* (Wiley, New York, 1984).

[3] P. Franken, A. E. Hill, C. E. Peters, and G. Weinreich, Generation of Optical Harmonics, Phys. Rev. Lett. **7**, 118 (1961).

[4] M. Celebrano, X. Wu, M. Baselli, S. Großmann, P. Biagioni, A. Locatelli, C. De Angelis, G. Cerullo, R. Osellame, B. Hecht *et al.*, Mode matching in multiresonant plasmonic nanoantennas for enhanced second harmonic generation, Nat. Nanotechnol. **10**, 412 (2015).

[5] A. Noor, A. R. Damodaran, I.-H. Lee, S. A. Maier, S.-H. Oh, and C. Ciracì, Mode-matching enhancement of second-harmonic generation with plasmonic nanopatch antennas, ACS Photon. **7**, 3333 (2020).

[6] M. Kauranen and A. V. Zayats, Nonlinear plasmonics, Nat. Photon. **6**, 737 (2012).

[7] Y. Kivshar, All-dielectric meta-optics and non-linear nanophotonics, Natl. Sci. Rev. **5**, 144 (2018).

[8] A. Krasnok, M. Tymchenko, and A. Alù, Nonlinear metasurfaces: A paradigm shift in nonlinear optics, Mater. Today **21**, 8 (2018).

[9] M. R. Shcherbakov, D. N. Neshev, B. Hopkins, A. S. Shorokhov, I. Staude, E. V. Melik-Gaykazyan, M. Decker, A. A. Ezhov, A. E. Miroshnichenko, I. Brener *et al.*, Enhanced third-harmonic generation in silicon nanoparticles driven by magnetic response, Nano Lett. **14**, 6488 (2014).

[10] S. Kruk, M. Weismann, A. Y. Bykov, E. A. Mamonov, I. A. Kolmychek, T. Murzina, N. C. Panoiu, D. N. Neshev, and Y. S. Kivshar, Enhanced magnetic second-harmonic generation from resonant metasurfaces, ACS Photon. **2**, 1007 (2015).

[11] S. Kim, J. Jin, Y.-J. Kim, I.-Y. Park, Y. Kim, and S.-W. Kim, High-harmonic generation by resonant plasmon field enhancement, Nature (London) **453**, 757 (2008).

[12] M. P. Nielsen, X. Shi, P. Dichtl, S. A. Maier, and R. F. Oulton, Giant nonlinear response at a plasmonic nanofocus drives efficient four-wave mixing, Science **358**, 1179 (2017).

[13] R. Czaplicki, A. Kiviniemi, M. J. Huttunen, X. Zang, T. Stolt, I. Vartiainen, J. Butet, M. Kuittinen, O. J. Martin, and M. Kauranen, Less is more: Enhancement of second-harmonic generation from metasurfaces by reduced nanoparticle density, Nano Lett. **18**, 7709 (2018).

[14] A. V. Krasavin, P. Ginzburg, and A. V. Zayats, Free-electron optical nonlinearities in plasmonic nanostructures: A review of the hydrodynamic description, Laser Photon. Rev. **12**, 1700082 (2018).

[15] M. Khalid and C. Ciracì, Enhancing second-harmonic generation with electron spill-out at metallic surfaces, Commun. Phys. **3**, 214 (2020).

[16] T. Shibanuma, G. Grinblat, P. Albella, and S. A. Maier, Efficient third harmonic generation from metal–dielectric hybrid nanoantennas, Nano Lett. **17**, 2647 (2017).

[17] O. Reshef, I. De Leon, M. Z. Alam, and R. W. Boyd, Nonlinear optical effects in epsilon-near-zero media, Nat. Rev. Mater. **4**, 535 (2019).

[18] A. D. Neira, N. Olivier, M. E. Nasir, W. Dickson, G. A. Wurtz, and A. V. Zayats, Eliminating material constraints for nonlinearity with plasmonic metamaterials, Nat. Commun. **6**, 7757 (2015).

[19] M. Z. Alam, I. De Leon, and R. W. Boyd, Large optical nonlinearity of indium tin oxide in its epsilon-near-zero region, Science **352**, 795 (2016).

[20] C. W. Hsu, B. Zhen, A. D. Stone, J. D. Joannopoulos, and M. Soljačić, Bound states in the continuum, Nat. Rev. Mater. **1**, 1 (2016).

[21] L. Carletti, K. Koshelev, C. De Angelis, and Y. Kivshar, Giant Nonlinear Response at the Nanoscale Driven by Bound States in the Continuum, Phys. Rev. Lett. **121**, 033903 (2018).

[22] K. Koshelev, S. Kruk, E. Melik-Gaykazyan, J.-H. Choi, A. Bogdanov, H.-G. Park, and Y. Kivshar, Subwavelength dielectric resonators for nonlinear nanophotonics, Science **367**, 288 (2020).

[23] J. B. Pendry, A. Aubry, D. Smith, and S. A. Maier, Transformation optics and subwavelength control of light, Science **337**, 549 (2012).

[24] A. Slablab, L. Le Xuan, M. Zielinski, Y. De Wilde, V. Jacques, D. Chauvat, and J.-F. Roch, Second-harmonic generation from coupled plasmon modes in a single dimer of gold nanospheres, Opt. Express **20**, 220 (2012).

[25] G.-C. Li, D. Lei, M. Qiu, W. Jin, S. Lan, and A. V. Zayats, Light-induced symmetry breaking for enhancing second-harmonic generation from an ultrathin plasmonic nanocavity, Nat. Commun. **12**, 4326 (2021).

[26] J. E. Sipe, V. C. Y. So, M. Fukui, and G. I. Stegeman, Analysis of second-harmonic generation at metal surfaces, Phys. Rev. B **21**, 4389 (1980).

[27] J. I. Dadap, J. Shan, K. B. Eisenthal, and T. F. Heinz, Second-Harmonic Rayleigh Scattering from a Sphere of Centrosymmetric Material, Phys. Rev. Lett. **83**, 4045 (1999).

[28] A. Capretti, C. Forestiere, L. Dal Negro, and G. Miano, Full-wave analytical solution of second-harmonic generation in metal nanospheres, Plasmonics **9**, 151 (2014).

[29] A. Aubry and J. B. Pendry, Transformation optics for plasmonics, in *Active Plasmonics and Tuneable Plasmonic Metamaterials* (John Wiley & Sons, Hoboken, NJ, 2013), pp. 105–152.

[30] K. N. Reddy, P. Y. Chen, A. I. Fernández-Domínguez, and Y. Sivan, Surface second-harmonic generation from metallic-nanoparticle configurations: A transformation-optics approach, Phys. Rev. B **99**, 235429 (2019).

[31] S. Elkabetz, K. N. Reddy, P. Y. Chen, A. I. Fernández-Domínguez, and Y. Sivan, Optimization of second-harmonic generation from touching plasmonic wires, Phys. Rev. B **103**, 075411 (2021).

[32] F. Yang, P. A. Huidobro, and J. B. Pendry, Transformation optics approach to singular metasurfaces, Phys. Rev. B **98**, 125409 (2018).

[33] C. Ciracì, E. Poutrina, M. Scalora, and D. R. Smith, Origin of second-harmonic generation enhancement in optical split-ring resonators, Phys. Rev. B **85**, 201403(R) (2012).

[34] C. Ciraci, E. Poutrina, M. Scalora, and D. R. Smith, Second-harmonic generation in metallic nanoparticles: Clarification of the role of the surface, Phys. Rev. B **86**, 115451 (2012).

[35] J. Pendry, P. A. Huidobro, Y. Luo, and E. Galiffi, Compacted dimensions and singular plasmonic surfaces, Science **358**, 915 (2017).

[36] M. Albooyeh, Electromagnetic characterization of metasurfaces, Ph.D. thesis, Aalto University, 2015.

[37] K. N. Reddy, P. Y. Chen, A. I. Fernández-Domínguez, and Y. Sivan, Revisiting the boundary conditions for second-harmonic generation at metal-dielectric interfaces, J. Opt. Soc. Am. B **34**, 1824 (2017).

[38] J. B. Pendry, D. Schurig, and D. R. Smith, Controlling electromagnetic fields, Science **312**, 1780 (2006).

[39] D. Schurig, J. Pendry, and D. R. Smith, Calculation of material properties and ray tracing in transformation media, Opt. Express **14**, 9794 (2006).

[40] Y. Luo, Transformation optics applied to plasmonics, Ph.D. thesis, Imperial College London London, UK, 2012.

[41] G. Arfken, H. Weber, and F. Harris, *Mathematical Methods for Physicists: A Comprehensive Guide* (Elsevier Science, Amsterdam, 2013).

[42] F. Yang, Y.-T. Wang, P. A. Huidobro, and J. B. Pendry, Nonlocal effects in singular plasmonic metasurfaces, Phys. Rev. B **99**, 165423 (2019).